

PRESERVATION OF A SUBDUCTION-RELATED GEOTHERMAL GRADIENT IN THE SCHIST OF SIERRA DE SALINAS, CENTRAL CALIFORNIA COAST RANGES

EMILY GROSS, Macalester College
Research Advisor: Alan Chapman

INTRODUCTION

Inverted metamorphic gradients in subduction complexes may be produced via multiple mechanisms. One possible explanation for inverted metamorphism is *en masse* underthrusting of sedimentary sequences. *En masse* underthrusting of cold sediments beneath a hot upper plate would lead to intense metamorphism at the upper plate-lower plate contact, with metamorphic grade decreasing with increasing structural depth (e.g., Ducea et al., 2009). Alternatively, the friction between upper and lower plates may explain inverted metamorphic sequences. A third possible explanation for inverted metamorphic gradients is sequential accretion of separate bodies below the upper plate (e.g., Kidder and Ducea, 2006; Grove et al., 2008).

The schist of Sierra de Salinas, located in the Coast Ranges of central California, displays an inverted metamorphic gradient. This inverted gradient was first described by Kidder and Ducea (2006) using garnet-biotite thermometry. Their work reveal peak temperatures that diminish with increasing structural depth from $>700\text{ }^{\circ}\text{C}$ to $\sim 575\text{ }^{\circ}\text{C}$. However, the mechanisms by which inverted metamorphism in the schist of Sierra de Salinas formed are not clear.

This project seeks to clarify the mechanisms by which the schist of Sierra de Salinas was assembled through U-Pb detrital zircon geochronology of samples collected over a range of structural depths, as each of the three mechanisms described above predict different age-depth relationships. Through geochronology and analysis of zoning in zircon grains, we were able to further define whether the schist of Sierra de

Salinas was accreted all at once or through sequential underplating.

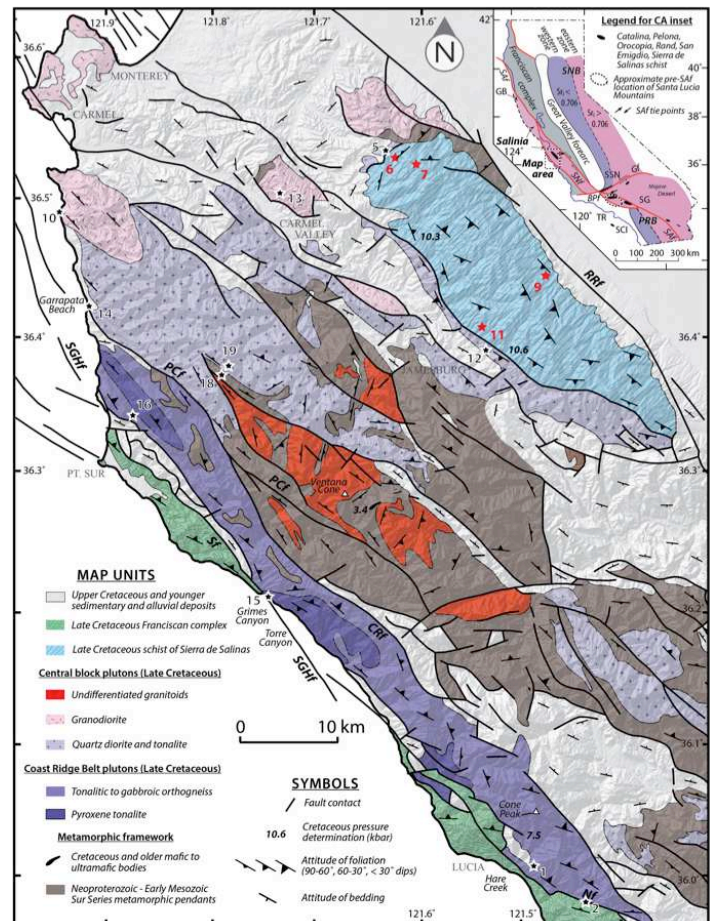


Figure 1. Map of Salina, with inlaid map of California, showing schist of Sierra de Salinas and sample sites (red labeled stars).

GEOLOGIC BACKGROUND

Salinia sits within the California Coast Ranges, bordered by the Big Pine fault in the south, the San Andreas fault in the east and the Sur-Nacimiento fault in the west (Hall, 1991). The Salinian block is underlain primarily by Late Cretaceous igneous and Mesozoic or older metamorphic basement rocks (Hall, 1991). In the last ca. 20 Ma, Salinia moved northwards along the San Andreas fault ~310 km (Miller et al, 1996).

The Santa Lucia Mountains sit along the coast of California, rising to about 1500m. Comprised of chiefly medium to high-grade metamorphic and granitic rocks, the Santa Lucia Mountains make up the largest metamorphic terrane within Salinia (Ross, 1979). The schist of Sierra de Salinas is within the Santa Lucia Mountains, in a structurally underthrust position beneath plutonic and metamorphic rocks of the Salinian block (Figure 1). The rocks of the Salinian block that the schist sit under are thought to correlate with the southernmost Sierra Nevada batholith. The schist was originally defined as a fairly monotonous metasandstone with some quartz veins and pegmatite (Ross, 1979). The schist is moderately west dipping, bounded by the Cretaceous Salinas shear zone in the west, which has been remobilized variably during the Neogene. The schist is bounded by the Neogene Reliz-Rinconada fault to the east. The schist of Sierra de Salinas belongs to a larger body of schists within California that include the Late Cretaceous Rand, Pelona and Orocopia schists (Figure 1 inset; Jacobson et al., 2000). These schists are widely regarded to have formed at the North America-Farallon plate margin during subduction. Detrital material was underplated along the Farallon plate, resurfacing after metamorphosing on the continental margin (Grove, 2003). The schist of the Sierra de Salinas is a prime example of this underplating.

METHODS

Detrital zircon grains were separated from samples collected along a cross section of the schist of Sierra de Salinas (See Figure 1). Samples underwent crushing, sieving, magnetic separation, processing through heavy liquids, and handpicking. Grains were then mounted in epoxy, polished, and imaged on a

scanning electron microscope at Macalester College before further analysis. Four samples were then analyzed by laser-ablation–multicollector–inductively coupled plasma–mass spectrometry (LA-MC-ICP-MS) at the Arizona LaserChron Center (ALC) following methods outlined in Gehrels et al. (2006). Zircon grains were ablated using a 193 nm ArF laser with a pit depth of ~12 microns and spot diameters of 15 microns, depending on grain size. Fragments of an in-house Sri Lanka (SL) zircon standard with an isotope dilution–thermal ionization mass spectrometry (ID-TIMS) age of 563.5 +/- 3.2 Ma (2σ) were analyzed once per every five unknown analyses to correct for instrument mass fractionation and drift (Gehrels et al., 2008). For three of the four samples, ~ten grains were analyzed by LA-MC-ICP-MS to determine differences in age between igneous cores and metamorphic zones and rims. The areas for analysis were determined using cathodoluminescence (CL) images taken with a SEM.

Normalized probability plots comparing analyzed samples were constructed with ALC Microsoft Excel programs using $^{207}\text{Pb}/^{206}\text{Pb}$ ages for grains older than 800 Ma and $^{206}\text{Pb}/^{238}\text{U}$ ages for grains younger than 800 Ma. Analyses with greater than 10% uncertainty, 30% discordance, and/or 5% reverse discordance were excluded. Weighted mean ages were calculated for each sample from weighted averages of youngest clusters that overlap within analytical uncertainty (discussed further below).

RESULTS

Of all the zircon grains analyzed, 338 grains yielded analyses below uncertainty and discordance thresholds for exclusion. Of the total grains analyzed, 59% yield Cretaceous ages, 12% yield Jurassic ages and the remainder yield Triassic and Proterozoic ages. Eleven percent of all analyzed grains yield an age of ca. 1.38 Ga (Figure 2). Of the four samples analyzed, SLM 6, 7 and 11 were located at higher structural depths, less than ~1 km from the upper plate bounding shear zone. In contrast, SLM 9 was located more than ~2km from the upper plate boundary, at lower structural depths. In the section that follows, I will contrast samples on the basis of the youngest populations of zircon grains

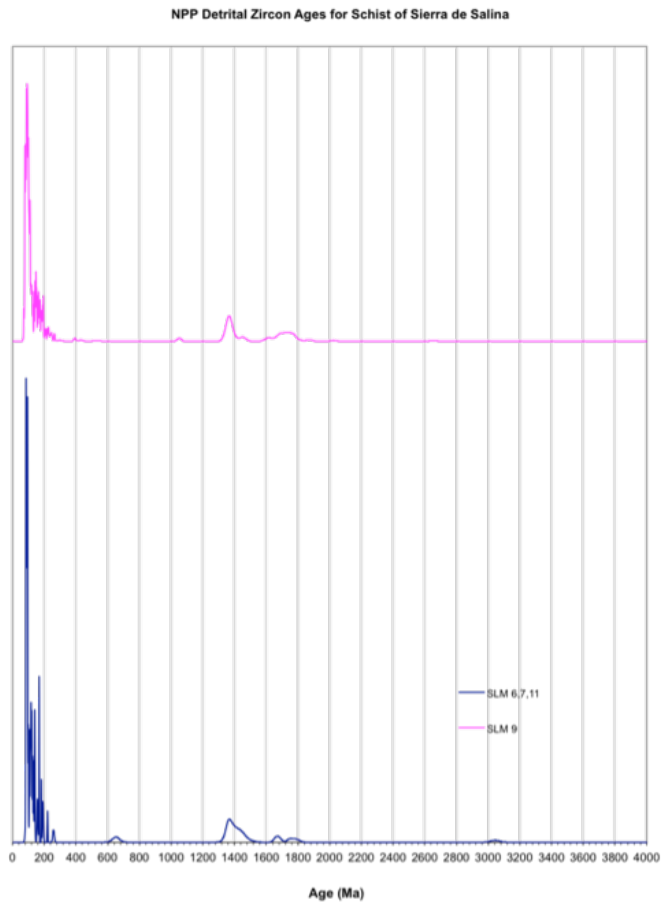


Figure 2. Normalized Probability Plot of ages, comparing peaks of structurally higher samples (SLM 6, 7, 11) with lower structural samples (SLM 9). Note the second peak at ca. 1.38 Ga.

present. Given that some of the youngest grains dated may be metamorphic in origin (i.e., not detrital), I will not use the common term “maximum depositional age,” instead defining the term “youngest age clusters (YACs),” as the latter avoids any genetic connotations.

Results for Structurally Deeper Sample

Sample SLM9 yielded ~60% Cretaceous zircon grains, and a YAC of 86 ± 2 Ma. Twenty percent of grains fell within this range. Of the remaining analyzed grains, 14% yielded ages within the range of ca. 1.38 Ga. Using cathodoluminescence (CL) imaging, we were able to find little evidence of metamorphism in most grains compared to other samples. Sample SLM 9 had fewer grains with extensive CL-bright rims, suggesting that nearly all analyzed grains had undergone minimal metamorphic recrystallization, relative to samples 6,7, and 11 (see below). These

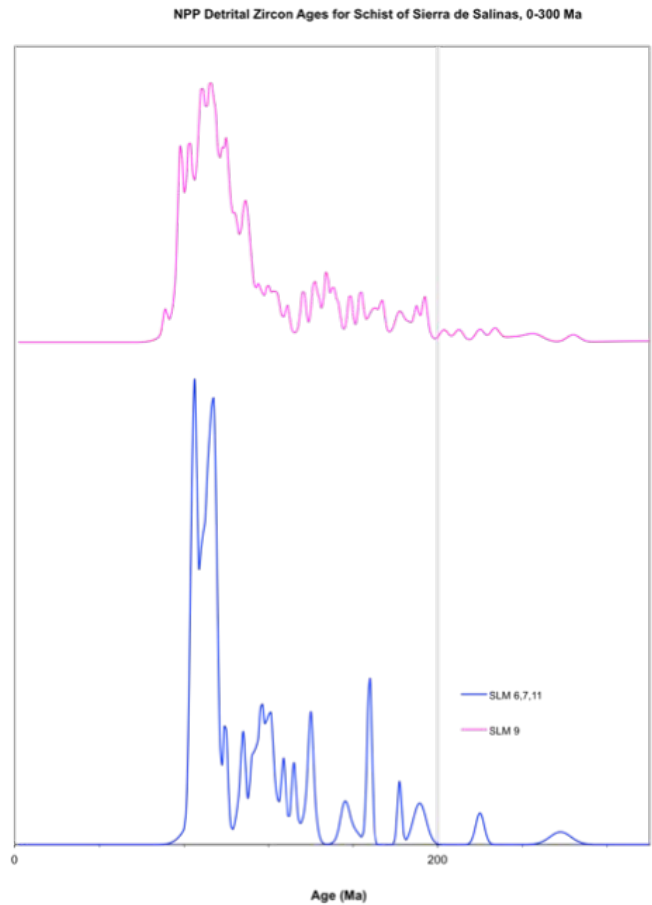


Figure 3. Normalized Probability Plot of ages from 0-300 Ma.

relations imply that most grains in sample SLM9 are detrital zircon.

Results for Structurally Higher Samples

Samples SLM 6, SLM 7, and SLM 11 were all located closer to the upper plate bounding shear zone, which means they formed at structurally higher levels than SLM 9. Sample SLM 7, located structurally the lowest of the three, yielded a YAC of 76 ± 2 Ma, with 10% of grains falling within this range. The majority (72%) of SLM 7 grains are Cretaceous, with 6% of the remaining grains yielding an age of ca. 1.38 Ga. A high percentage of grains in sample SLM 7 display CL-bright rims that truncate interior core zones. These rim domains are probably metamorphic zircon that overgrew detrital igneous core domains (Figure 4).

Of sample SLM11 grains analyzed, 48% yield Cretaceous ages and 9% of grains fall within the ca. 1.38 Ga age range. Zircon grains from sample SLM11 yield a YAC of 78 ± 4 Ma. Like sample SLM 7, zircon grains from sample SLM11 also show significant CL bright-rims, like the ones shown in Figure 4 that have a total thickness of nearly 90 μm .

Sample SLM 6, the structurally shallowest sample taken, contains 56% Cretaceous aged grains; 13% of SLM6 grains yield an age of ca. 1.38 Ga. SLM6 grains yield a YAC of 78 ± 3 Ma, with 16% of total grains included in this average. Like samples SLM7 and SLM11, sample SLM6 also contains CL-bright rims on a large number of the grains analyzed (Figure 4).

The ages of the three samples that formed structurally higher within the schist, when considered as one group, yield a YAC of 77 ± 3 Ma. Of all grains of the three samples, 9% fall within this average (Figure 3).

DISCUSSION

All analyzed samples contain abundant Cretaceous detrital zircon grains, with diminishing proportions of Jurassic, Triassic, and Proterozoic grains, consistent with a Sierra Nevada arc source (Grove et al. 2003; Jacobson et al. 2011). Also noteworthy are the $\sim 11\%$ of total dated grains yielding ages of ca. 1.38 Ga, which require subsidiary input from detrital sources outside of the Sierran arc, as zircon grains of this age are cited as originating from Idaho or the Mojave Desert (Garver and Davidson, 2015; Dumitru et al., 2016).

Our results show that the schist was probably not

assembled through sequential underplating. The results yield YACs that suggest upsection younging, with older samples at lower structural depths. If sequential underplating had occurred, we would expect to observe downsection younging. Observed upsection younging may be explained in three ways: 1) the schist may represent a subducted but otherwise intact stratigraphic section, 2) recrystallization of metamorphic zircon occurred within the Sierran arc, and/or 3) recrystallization of metamorphic zircon occurred in the subduction zone. When correlated with existing thermobarometric constraints, we see that samples yielding younger culsters of ages are structurally higher and hence reached peak temperatures of >700 $^{\circ}\text{C}$ (Kidder and Ducea, 2006). The structurally deepest sample (SLM9), with older ages, correlate with lower temperatures of about to ~ 575 $^{\circ}\text{C}$.

We consider the scenario of the schist as a subducted but intact stratigraphic section unlikely. If the schist were an intact sedimentary section, we would expect to see younging as we moved higher structurally across section. We do observe younger ages at higher structural depths, but the higher proportion of CL-bright zircon rims in the samples with 77 ± 3 YACs suggest that these grains are not detrital. If the grains are not detrital they are not recording the maximum depositional age, but rather the age of metamorphic crystallization.

Scenario 2, where recrystallization of metamorphic zircon occurred within the Sierran arc, is suspect because magmatism in the Sierran arc shut off by ca. 84 Ma and no ca. 77 Ma metamorphic episodes are recognized within the arc (e.g. Chen and

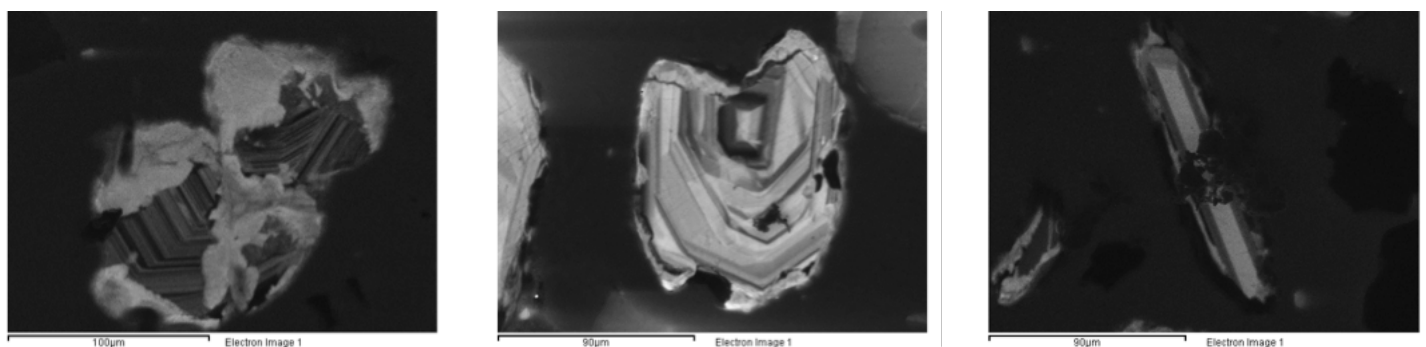


Figure 4. CL images of zircon grains from samples SLM6, SLM11 and SLM7 respectively, showing metamorphic zonation. The bright rims and zones in the grains are areas of assumed metamorphic recrystallization.

Moore, 1982). Furthermore, if ca. 77 Ma zircon recrystallization occurred in the Sierran arc, significant quantities of these grains would be expected throughout the broadly correlative Pelona-Orocopia-Rand schist outcrop belt, for which little evidence exists (Grove et al., 2003; Jacobson et al., 2011).

We favor scenario 3 because recrystallized zircon is abundant at the highest structural levels where the highest peak temperatures are reported and partial melting has taken place, suggesting a possible causative relationship. In this scenario, peak temperatures in areas of higher structural depth can be explained by underplating of the schist, as described by Ducea et al (2009).

CONCLUSION

We conclude that the schist of Sierra de Salinas was sourced primarily from the Sierra Nevada batholith and adjacent areas. The ~11% of grains that yield an age of ca. 1.38 Ga may also have been derived from the Mojave Desert, south of the Sierra Nevada, where grains of this rare age are reported (Garver and Davidson, 2015). However, we cannot rule out the possibility that these grains originated from central Idaho, as Dumitru et al. (2016) suggests.

We also conclude that the structurally deepest levels of the schist of Sierra de Salinas, and perhaps the schist as a whole, were deposited after 86 ± 2 Ma and emplaced en masse beneath a hot upper plate at 77 ± 3 Ma, forming an inverted metamorphic record of the geothermal gradient that existed during subduction.

ACKNOWLEDGEMENTS

I was able to conduct this research thanks to a grant from the Keck Geology Consortium. I would like to thank my project advisor Alan Chapman and Keck advisor Sarah Brownlee. I would also like to thank all my fellow Keck students for their help and camaraderie in the field. Also, thank you to the University of Arizona Laserchron Center and Macalester College for access to their facilities. A final thanks goes to the Landels-Hill Big Creek Reserve (UCSC), the Hastings Natural History Reservation (UC Berkeley), and private landowner Steve Dorrance,

for granting access to private property during this project.

REFERENCES

- Chen, J.H., and Moore, J.G., 1982, Uranium-lead isotopic ages from the Sierra Nevada batholith, California: *Journal of Geophysical Research*, 87, 4761–4784
- Dickinson, W.R., and Gehrels, G.E., 2009, U-Pb ages of detrital zircons in Jurassic eolian and associated sandstones of the Colorado Plateau: Evidence for transcontinental dispersal and intraregional recycling of sediment: *GSA Bulletin*, 121, 408–433
- Ducea, M. N., S. Kidder, J. T. Chesley, and J. B. Saleeby, 2009, Tectonic underplating of trench sediments beneath magmatic arcs: the central California example: *International Geology Review*, 51, 1-26
- Dumitru, T. A., Elder, W. P., Hourigan, J. K., Chapman, A. D., Graham, S. A., and Wakabayashi, J., 2016, Four Cordilleran paleorivers that connected Sevier thrust zones in Idaho to depocenters in California, Washington, Wyoming, and, indirectly, Alaska: *Geology*, 44, 75–78, doi:10.1130/G37286.1.
- Garver, J., and Davidson, C., 2015, Southwestern Laurentian zircons in upper Cretaceous Flysch of the Chugach-Prince William terrane in Alaska: *American Journal of Science*, 315, 537-556
- Grove, M., Jacobson, C.E., Barth, A.P., and Vucic, A., 2003, Temporal and spatial trends of Late Cretaceous –early Tertiary underplating of Pelona and related schist beneath southern California and Southwestern Arizona: Tectonic evolution of northwestern Mexico and the southwestern USA, 374, 381.
- Grove, M., Bebout, G.E., Jacobson, C.E., Barth, A.P., Kimbrough, D.L., King, R.L., Zou, H., Lovera, O.M., Mahoney, B.J., and Gehrels, G.G., 2008, The Catalina schist: Evidence for middle Cretaceous subduction erosion of southwestern North America, in Draut, A.E., Cliff, P.D., and Scholl, D.W., eds., *Formation and Applications of the Sedimentary Record in Arc Collision Zones: Geological Society of America Special Paper*, 436, 335–362

- Gehrels, G., Valencia, V., and Pullen, A., 2006, Detrital zircon geochronology by laser-ablation multicollector ICPMS at the Arizona Laserchron Center: *The Paleontological Society Papers*, 12, 67–76.
- Gehrels, G., Valencia, V.A., and Ruiz, J., 2008, Enhanced precision, accuracy, efficiency, and spatial resolution of U-Pb ages by laser ablation–multicollector–inductively coupled plasma–mass spectrometry: *Geochemistry Geophysics Geosystems*, 9, 3
- Hall, C.A., Jr., 1991, *Geology of the Point Sur–Lopez Point region, Coast Ranges, California: A part of the Southern California allochthon: Geological Society of America Special Paper 266*, 44
- Jacobson, C. E., A. P. Barth, and M. Grove, 2000, Late Cretaceous protolith age and provenance of the Pelona and Orocopia Schists, southern California: Implications for evolution of the Cordilleran margin: *Geology*, 28, 219
- Jacobson, C.E., Grove, M., Pedrick, J.N., Barth, A.P., Marsaglia, K.M., Gehrels, G.E., and Nourse, J.A., 2011, Late Cretaceous–early Cenozoic evolution of the southern California margin inferred from provenance of trench and forearc sediments: *Geological Society of America Bulletin*, v. 123, no. 3–4, p. 485–506
- Kidder, S., and Ducea, M.N., 2006, High temperatures and inverted metamorphism in the schist of Sierra de Salinas, California: *Earth and Planetary Science Letters*, 241, 422–437
- Miller, J.S., Glazner, A.F., and Crowe, D.E., 1996, Muscovite-garnet granites in the Mojave Desert: Relation to crustal structure of the Cretaceous arc: *Geology*, 24, 335–338.
- Ross, D., 1979, *Reconnaissance geologic map of Pre-Cenozoic basement rocks northern Santa Lucia range, Monterey County, California: United States Geological Survey*